# Pressure dependence of the structure of liquid NiTi: a molecular dynamics study

*by* Ghulam Buntoro

**Submission date:** 11-Oct-2019 12:29PM (UTC+0700)
**Submission ID:** 1190634705
**File name:** of_the_structure_of_liquid_NiTi-_a_molecular_dynamics_study.pdf (1.96M)
**Word count:** 4594
**Character count:** 21104

IOP Publishing Journal of Physics: Condensed Matter
J. Phys.: Condens. Matter **31** (2019) 365401 (8pp) https://doi.org/10.1088/1361-648X/ab25b4

# Pressure dependence of the structure of liquid NiTi: a molecular dynamics study

**Rizal Arifin[1,4], Muhammad Malyadi[1], Munaji[1], Ghulam Asrofi Buntoro[2] and Darminto[3]**

[1] Department of Mechanical Engineering, Universitas Muhammadiyah Ponorogo, Jl. Budi Utomo No. 10 Ponorogo, 63471 Indonesia
[2] Department of Informatics Engineering, Universitas Muhammadiyah Ponorogo, Jl. Budi Utomo No. 10 Ponorogo, 63471 Indonesia
[3] Department of Physics, Institut Teknologi Sepuluh Nopember, Kampus ITS Sukolilo Surabaya, 60111 Indonesia

E-mail: rarifin@umpo.ac.id

Received 28 January 2019, revised 22 May 2019
Accepted for publication 30 May 2019
Published 21 June 2019

**Abstract**

We evaluate the structure of liquid NiTi under various pressures from 0 GPa to 40 GPa in the atomic level using molecular dynamics simulations. The structure factor and radial distribution function are used to investigate the general structural change of the system. Further identification of the local structures is examined by the bond-angle method and bond-angle distribution analysis. From our results, we found that the count of the local structure of fcc, hcp, bcc, and icosahedral short-range order monotonically increase when the pressures increase. We also observed in our results that the size of the local cluster grows as the pressure increases, and the long-range connectivity of the quasi-crystal is achieved at high pressure.

Keywords: molecular dynamics simulations, liquid NiTi, pressure, local structures

Supplementary material for this article is available online

(Some figures may appear in colour only in the online journal)

## 1. Introduction

The structure of liquid metal in various thermodynamic conditions has attracted much interest from researchers over the past decades [1–5]. To produce multi-component metal alloys, monoatomic metals are usually mixed in their liquid state before undergoing crystal growth during the solidification processes. The heterogeneity of atomic distribution [6, 7] in the liquid state, the thermodynamic conditions [8], and the quenching rate [9, 10] may affect the mechanical properties of solid material. Thorough investigation of the liquid structure under various thermodynamic conditions is indispensable to reveal its structural properties. It is known from experiments that the structure of liquid metals and amorphous metals have similar general features; for example, shoulders or the splitting of the second peak observed in the structure factor [11]. Molecular dynamics (MD) simulation can produce a realistic model at the atomic level to provide more detailed structural properties of liquid. Li *et al* studied liquid and amorphous Al using classical MD simulation [12], while Jakse and Pasturel performed *ab initio* MD simulation of atomic diffusion and the viscosity of liquid Al [13]. Structural investigation of liquid Te using MD simulation was conducted by Hoshino [14], and recently, Wu *et al* observed some fluctuation and competition between icosahedral and bcc in undercooled liquid Zr [15]. Although some MD studies of liquid metals have been made, to the best of our knowledge no previous paper has studied liquid NiTi alloy. NiTi exhibits shape memory effect (SME) property, therefore it is categorized as a shape memory alloy (SMA) material. This material can undergo the deformation and then recover to its original shape above the transition temperature [16, 17]. NiTi alloy is a biocompatible material which is highly elastic. This material also has the extreme corrosion and kink resistances [18–20]. By these attractive properties, NiTi alloy is widely used as a biomaterial, such as orthodontic arch wire, bone anchor, and stents [21]. NiTi

[4] Author to whom any correspondence should be addressed.

 

alloy is also known to be an expensive material due to its difficult fabrication process, therefore it is very important to have comprehensive information on the alloy from the liquid to the solid state. In the initial state of NiTi fabrication, the pure Ni and Ti metals are mixed by the atomic ratio of 50:50 in the liquid phase. The presence of the pressure during the fabrication will indeed affect the structure of the liquid and solid NiTi alloy. In this paper, we present the results of the structural analysis of liquid NiTi at the atomic level under various pressures. The study aims to elucidate the structural change in liquid NiTi when various pressures are applied to the system. The result of this investigation can be utilized to predict the structure of the quenched NiTi product.

## 2. Method of calculation

We carried out the MD calculation using the large-scale atomic/molecular massively parallel simulator (LAMMPS) package [22]. The interactions between Ni–Ni, Ni–Ti and Ti–Ti atoms were described by the embedded-atom method (EAM) potential by Zhou et.al. [23], which has been well tested for high-temperature MD simulations [24]. From our previous preliminary calculation, the EAM potential used in this simulation has successfully reproduce the melting point of the eutectic NiTi alloy using two-phase approach with the high accuracy of 94.76% [24]. Figure 1 shows the initial configuration of the simulation system containing 16 000 atoms (8000 atoms for both Ni and Ti). It can be seen from figure 1 that he initial structure is in liquid phase. It was prepared by heating up the B2 structure of NiTi alloy from 300 K to 2500 K. Periodic boundary conditions were applied in the cubic supercell with dimensions of 64.874 × 64.874 × 64.874 Å$^3$. The equations of motion were numerically solved using the Verlet algorithm with a time step of $\Delta t = 1$ fs and the NPT Nosé–Hoover technique [25, 26] was employed to equilibrate the system at 2500 K (0 GPa) for 100 ps. Further equilibration processes were then performed at 10, 20, 30, and 40 GPa for another 100 ps in order obtain the final configuration of the NiTi alloy system in the different pressure conditions. Figures 2(a) and (b) shows the plot of the energy and the pressures, respectively, during the equilibration time of 100 ps for two different pressures of 0 GPa and 30 GPa. It can be seen clearly that the total energy, kinetic energy, and the pressures are converged to the certain values.

We extracted the data from the extended MD simulation using the NVT ensemble after equilibration was carried out for 50 ps. The convergence of the energy and the pressures during the production time are shown in figures 2(c) and (d). Structural analysis was then performed using the Rings package [27], with the atomic visualization image rendered in Ovito [28].

## 3. Results and discussion

For the respective pressures $P$, the change of the atomic densities $\rho$ and the volume ratio $V/V_0$, where $V_0$ is the volume at the ambient pressure, are listed in table 1. The atomic density increase and the volume shrink when the pressures increase.

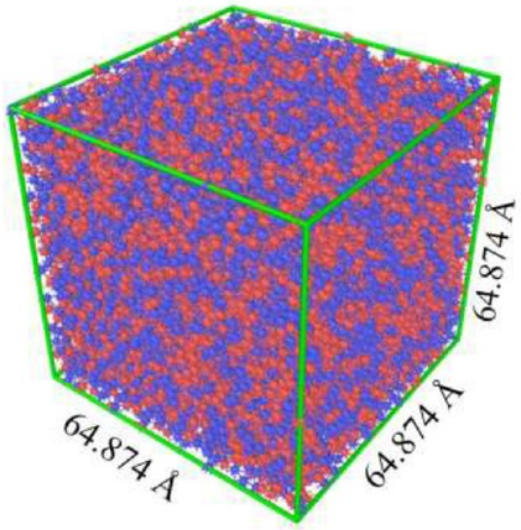


**Figure 1.** Initial configuration of liquid NiTi alloy at $T = 2500$ K. The red and the blue balls correspond to the Ni and the Ti atoms respectively. The system consists of 8000 Ni atoms and 8000 Ti atoms.

### 3.1. Structure factor of liquid Ni, Ti and NiTi alloy

To analyze the structural dependence of the pressure, we first obtained the static structure factor using the Ashcroft–Langreth formalism as follows:

$$S(q) = \frac{\sum_{\alpha,\beta} b_\alpha b_\beta (c_\alpha c_\beta)^{1/2} \left[S^{AL}_{\alpha\beta}(q) + 1\right]}{\sum_\alpha c_\alpha b_\alpha^2},$$

where $b_\alpha$ and $b_\beta$ are the x-ray form factors for atoms $\alpha$ and $\beta$, and $c_\alpha$ and $c_\beta$ are the concentrations of the two atoms. $S^{\mathrm{AL}}_{\alpha\beta}(q)$ is the partial structure factor defined by:

$$S^{\mathrm{AL}}_{\alpha\beta}(q) = \delta_{\alpha\beta} + 4\pi\rho(c_\alpha c_\beta)^{1/2} \int_0^\infty dr r^2 \frac{\sin qr}{qr} \left(g_{\alpha\beta}(r) - 1\right),$$

where $\delta_{\alpha\beta}$ is Kronecker delta and the $g_{\alpha\beta}(r)$ is the partial radial distribution functions.

Figure 3 shows the structure factor of liquid Ni and liquid Ti at temperatures of $T = 1769$ K and $T = 1973$ K respectively. The results were obtained at ambient pressures. From the figure, we can see that our results (solid black lines) agree with the previous experimental results shown in red circles [29]. The positions of the main peaks obtained from our MD simulation fit very well with the experimental data. At the larger $q$, the experimental $S(q)$s is slightly higher than that from our results. However, it can be clearly seen that the patterns are identical, indicating that the physical properties are the same. The slight differences may come from the system size effect, as the size

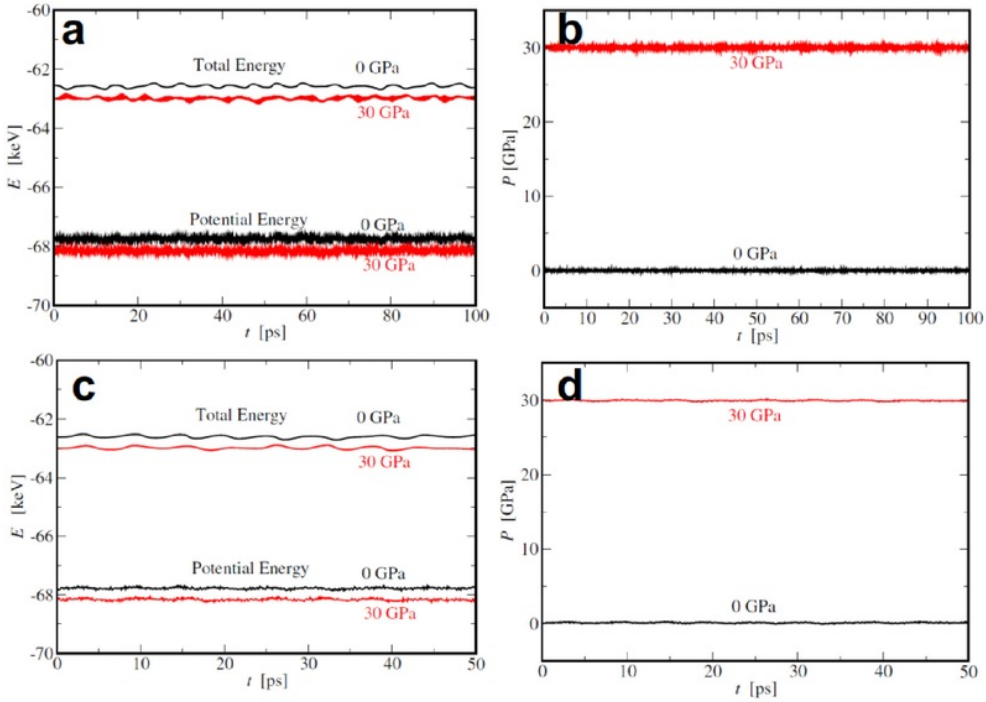


**Figure 2.** Time evolution of three properties of the system during the equilibration and the production time. (a) Total and potential energies and (b) pressures of the system during the equlibration of 100 ps in the NPT ensembel. The same properties of (a) and (b) are presented in (c) and (d), respectively, during the production of 50 ps in the NVT ensembel. The black and the red lines correspond to the result from the system under the pressure of 0 GPa and 10 GPa, respectively.

**Table 1.** Values of the atomic density $\rho$ and relative volume $V/V_0$ at $T = 2500$ K under pressures of 0, 10, 20, 30 and 40 GPa.

| $P$ (GPa) | $\rho$ ($10^{-2}$ Å$^{-3}$) | $V/V_0$ |
|---|---|---|
| 0 | 5.86 | 1.00 |
| 10 | 6.64 | 0.88 |
| 20 | 7.24 | 0.81 |
| 30 | 7.69 | 0.76 |
| 40 | 8.08 | 0.73 |

of the experimental samples is quite large compared with those of the simulation system. In this paper, we are unable to show a comparison of the liquid NiTi structure factor, since to the best of our knowledge liquid NiTi experimental data are currently unavailable. In order to evaluate the effect of the simulation system size of NiTi alloy, we have calculated the average total energy per atom and obtained the structure factor $S(q)$ from different simulation system size. We find that the value of the total energy per atom in our current simulation system of NiTi, containing 16 000 atoms in total, is almost the same with the simulation system of 31 250 atoms (see figure S1 in supplementary material (available online at stacks.iop.org/JPhysCM/31/365401/mmedia)). The clear prepeak is observed in the $S(q)$ of simulation system with 250 atoms, however, this property disappears in the larger simulation systems (see figure S2 in supplementary material). It is also found that $S(q)$ of the simulation system with 16 000 and 31 250 atoms are very

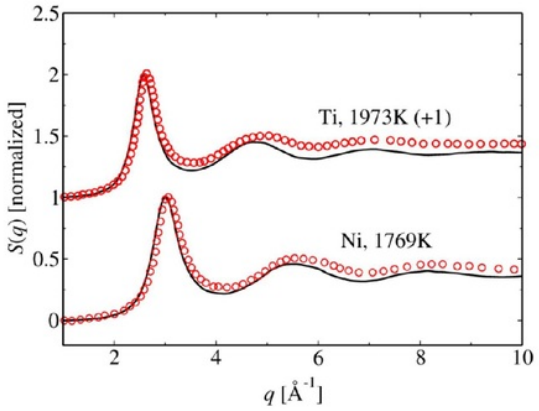


**Figure 3.** Normalized structure factor $S(q)$ of liquid Ni ($T = 1769$ K) and liquid Ti ($T = 1973$ K). The solid black lines and red circles correspond to the results from this research and from a previous experiment [29], respectively.

similar, which indicate the convergence of the results. From these results, we are convinced that our simulation system size is sufficient for this MD simulation.

Figure 4 shows the pressure dependence of the liquid NiTi total structure factor $S(q)$. It can be seen that the position of the first peak shifts slightly towards the higher $q$ value when

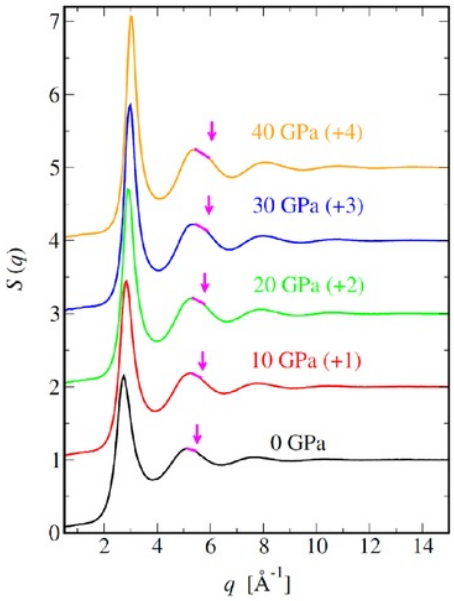


**Figure 4.** Total structure factor $S(q)$ of liquid NiTi ($T = 2500$ K) under pressures of 0, 10, 20, 30 and 40 GPa. The pink arrows point to the shoulders, which is marked using pink lines, at the higher $q$ of the second peaks.

the pressure is increased. In the figure, the presence of a first sharp diffraction peak (FSDP) at all pressures is not observed. On the other hand, shoulders appear on the right-hand side of the second peaks and can be seen more clearly at higher pressures. According to previous studies, a shoulder on the right-hand of the second peaks indicates the existence of the local icosahedral short-range order (ISRO) [30–32]. We have also calculated the $S(q)$ of the icosahedral $Ni_{13}$ cluster at various temperatures, i.e. 500 K, 700 K, 900 K, and 1100 K. We find that the shoulder of the second peak exhibits clearly in the low temperature of 500 K and 700 K (see figure S3 in supplementary material). In the high temperature of 900 K and 1100 K, the second peak and the shoulder appearance are weakened by the distortion of the icosahedral structure, as it is observed in our MD simulation of NiTi alloy. These results provide the direct evidence that the shoulder of the second peaks of $S(q)$ correspond to the presence of icosahedral structure.

We further quantify the $S(q)$ by identifying the locations of the first peak $q_{1st}$, the second peak $q_{2nd}$, and the shoulder $q_{shoulder}$ of each pressure $P$, which are listed in table 2. In this table, we also present the quantitative values of $q_{2nd}/q_{1st}$ and $q_{shoulder}/q_{1st}$. The existence of the ISRO has been theoretically identified by the values of 1.71 and 2.04 for $q_{2nd}/q_{1st}$ and $q_{shoulder}/q_{1st}$, respectively [31, 33]. When the pressure increases, it can be seen clearly from table 2 that the values of the $q_{2nd}/q_{1st}$ and $q_{sh}/q_{1st}$ become closer to the theoretical ones

**Table 2.** Values of the locations of the first peak $q_{1st}$, the second peak $q_{2nd}$, and the shoulder $q_{sh}$ with their ratio of $q_{2nd}/q_{1st}$ and $q_{sh}/q_{1st}$ at $T = 2500$ K under pressures of 0, 10, 20, 30 and 40 GPa.

| $P$ (GPa) | $q_{1st}$ (Å$^{-1}$) | $q_{2nd}$ (Å$^{-1}$) | $q_{sh}$ (Å$^{-1}$) | $q_{2nd}/q_{1st}$ | $q_{sh}/q_{1st}$ |
|---|---|---|---|---|---|
| 0 | 2.74 | 5.08 | 5.48 | 1.85 | 2.00 |
| 10 | 2.84 | 5.14 | 5.66 | 1.81 | 1.99 |
| 20 | 2.89 | 5.19 | 5.79 | 1.80 | 2.00 |
| 30 | 2.94 | 5.24 | 5.88 | 1.78 | 2.00 |
| 40 | 2.99 | 5.29 | 6.01 | 1.76 | 2.01 |

for ISRO. This result indicates that the count of ISRO grows with increasing pressures.

### *3.2. Radial distribution function of liquid NiTi under different pressures*

We present the total radial distribution function $g(r)$ of liquid NiTi in order to explain its real-space information. Figure 5(a) shows the pressure dependence of the radial distribution function. The smooth convergence of the total radial distribution function at a higher $r$ value suggests the random distribution of the atoms in the liquid system. It can be clearly seen in the figure that the first, second and third peaks shift to the left. The intensity of the peaks also increases when the pressure is higher.

The heights of the first, second and the third peaks for each pressure (0, 10, 20, 30 and 40 GPa) are shown in figure 5(b). The height (peak intensity) is calculated as the vertical distance between a peak and its previous valley. From the figure, it can be seen that the height of the three peaks increases with increased pressure. It is also shown that the most significant change in height is found when the pressure was raised from 30 GPa to 40 GPa. This result suggests that the fraction of local structures is considerably higher at 40 GPa and at a temperature of 2500 K. Figure 5(c) shows the change in position of the second and third peaks. From the figure, it can clearly be seen that the position of the second and third peaks moves towards a lower $r$ value with an increase in pressure. The lower $r$ value of the peak position suggests that the distance between the atoms becomes shorter and that the atoms are packed more densely. The similar features are found in the partial radial distribution functions. Figure 6 shows the partial radial distribution function of Ni–Ni $g(r)_{NiNi}$. When the pressure increases, the position of the first and the second peaks are shifted from the higher $r$ to the lower $r$, as expected for the densification. At 0 GPa, the first nearest neighbors are located in the $r_{1st}$ equal to 2.46 Å, 2.61 Å, and 2.80 Å for Ni–Ni, Ni–Ti, and Ti–Ti pairs, respectively. The second neighbors of Ni–Ni, Ni–Ti, and Ti–Ti pairs are in the distance ($r_{2nd}$) of 4.91 Å, 5.07 Å, and 5.19 Å, respectively. We found at 40 GPa that the values of the $r_{1st}$ are 2.27 Å, 2.45 Å, and 2.67 Å for Ni–Ni, Ni–Ti, and Ti–Ti pairs, respectively. It is also found

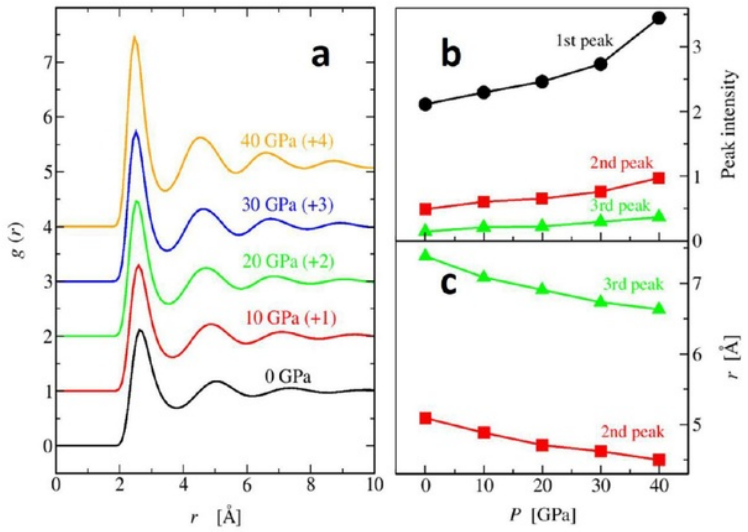


**Figure 5.** Structural analysis of the liquid NiTi at 2500 K under pressures of 0, 10, 20, 30 and 40 GPa. (a) radial distribution function $g(r)$ of liquid NiTi; (b) intensity of the first, second and third peaks of the $g(r)$ plot; and (c) position of the second and third peaks of the $g(r)$ plot.

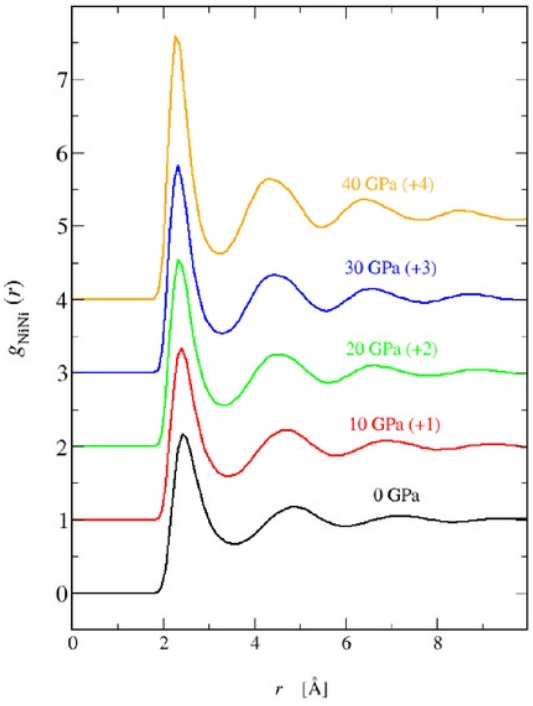


**Figure 6.** Partial radial distribution function $g(r)$ of liquid NiTi ($T = 2500$ K) under pressures of 0, 10, 20, 30 and 40 GPa.

that at 40 GPa, the values of $r_{2nd}$ of Ni–Ni, Ni–Ti, and Ti–Ti pairs are 4.32 Å, 4.51 Å, and 4.68 Å, respectively.

### *3.3. Bond angle distribution of liquid NiTi under different pressures*

We further evaluated the bond-angle distribution of the liquid NiTi system in order to characterize the local structure in a higher order correlation. The bond-angle distribution of the three atomic correlations is shown in figure 7. The partial bond-angle distribution of Ni–Ni–Ni and Ti–Ti–Ti show two main peaks at 55 degrees (1st) and 100 degrees (2nd) at 40 GPa. The Ni–Ni–Ni angular position of the 1st peak differs by around 5 degrees from that one at 0 GPa. The height of the 2nd peak at 40 GPa also higher by 0.1% than that one at 0 GPa. For other atomic combinations, the clear difference between the bond angle distribution of the system at 0 GPa and 40 GPa are observed at the minimum, height of the second peaks, and the growth of its shoulder. It was also found that at 40 GPa that the bond-angle of Ni–Ni–Ti exhibits peaks at 55 and 105 degrees. These results suggest the presence of a bcc-like structure, with a high probability at around 53 degrees. The bond-angle distribution of Ti–Ni–Ti has two main peaks at 60 and 105 degrees. 60 degrees corresponds to the fcc, hcp or ISRO [34]. Two main peaks at 50 and 100 degrees are found in the bond-angle distribution of Ti–Ti–Ni and Ni–Ti–Ni, deviating from the typical local structure of bcc, fcc and hcp. At higher pressure, the quasi-flats are formed at around 150 degrees. This indicates the formation of complex tetrahedral structures [34].

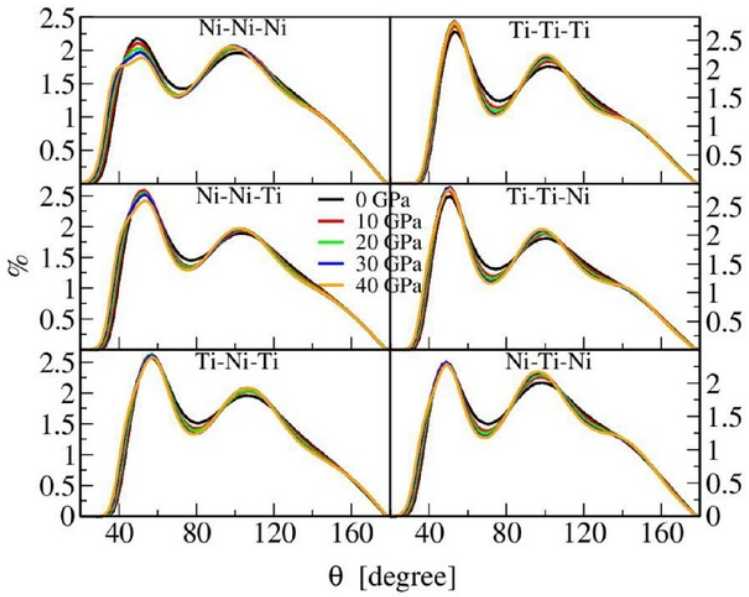


**Figure 7.** Bond angle distribution of liquid NiTi at 2500 K. The black, red, green, blue and orange lines correspond to the system results under pressures of 0, 10, 20, 30 and 40 GPa respectively.

**Table 3.** Count of the local atomic packing which is calculated using bond-angle method [35] at $T = 2500$ K under pressures of 0, 10, 20, 30 and 40 GPa.

| *P* (GPa) | fcc (%) | hcp (%) | bcc (%) | ISRO (%) |
|---|---|---|---|---|
| 0 | 0.7 | 12.8 | 8.6 | 0.3 |
| 10 | 1.2 | 17.7 | 13.0 | 0.5 |
| 20 | 1.5 | 21.5 | 16.1 | 0.8 |
| 30 | 1.9 | 23.3 | 17.4 | 1.0 |
| 40 | 2.3 | 24.5 | 19.0 | 1.5 |

### *3.4. Local atomic packing of liquid NiTi under different pressures*

The bond-angle analysis method [35], which focuses on angular distribution of local neighboring for each individual atom, was used to investigate the presence of the icosahedral local structure in our liquid NiTi system. This method is designed only for a monatomic system. Therefore, we performed the analysis on all of the atoms in our system without differentiating between the Ni and Ti atoms. The results of the bond-angle analysis for the local fcc, hcp, bcc, and ISRO are shown in table 3. At a pressure of 0 GPa, only 0.3% atoms are identified as ISRO local structure. Since the count of this structure is quite small, therefore of the shoulder of the second peak of structure factor (see figure 4) is also unclear. At higher pressures, the ISRO count increases up to 1.5% at 40 GPa of pressure. It can be seen clearly in table 3 that the count of fcc, hcp, and bcc like structure are also increase monotonically when the pressure increases. The highest proportion of local atomic packing is found as the hcp structure. The presence of fcc, hcp, bcc, and ISRO local atomic packing is consistence with the results from the bond-angle distribution analysis.

The graphics output of the configuration of bcc and ISRO local structures are shown in figure 8. The bonds are drawn between the atoms separated by the distance less than 3.8 Å, which is obtained from the first minimum of $g(r)$ at ambient pressure. The bulks are then sliced by the thickness of 6.20 Å described from the second minimum of the $g(r)$ at ambient pressure. It can be observed graphically from figures 8(a)–(e) that the long-range connectivity of the quasicrystal is achieved at the high pressure. We can see that as the pressure increase, the maximum cluster size grows through the precipitation of the individual and small local cluster. In this sliced region, the number of connected atoms in the local cluster are 8, 9, 17, 63, and 66 for the system under the pressure of 0, 10, 20, 30, and 40 GPa, respectively.

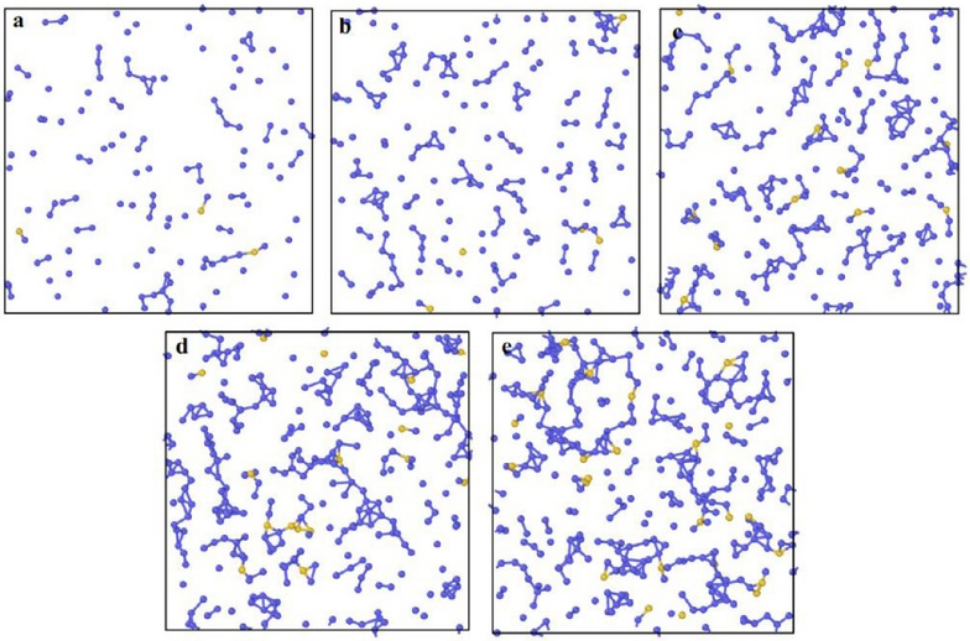


**Figure 8.** Snapshot of the configuration of the selected local atomic packing for (a) 0 GPa, (b) 10 GPa, (c) 20 GPa, (d) 30 GPa, and (e) 40 GPa. Only the atoms correspond to the bcc and ISRO local structure are shown for the clarity. The systems are sliced by the thickness of 6.20 which is the value of the second minimum of $g(r)$. The blue and yellow balls correspond to the bcc and ISRO local structures, respectively.

## 4. Conclusion

The pressure dependence of the liquid NiTi structure has been studied using MD simulations. These were performed at a temperature of 2500 K under pressures of 0, 10, 20, 30 and 40 GPa. From the total structure factors and bond-angle method, we ascertained the local ISRO structure in the liquid NiTi system. We also clarified that the fcc, hcp, bcc, and ISRO local structure increases monotonically when a higher pressure is applied to the system. From the radial distribution functions, we also found that the peak positions shift to the lower $r$-value and become higher with an increase of the pressure. These results suggest that some local structures are formed in the densely packed system. In addition to the ISRO, some signs of other local structures are also suggested by bond-angle distributions. The results indicate the existence of fcc-, hcp-, bcc-, and hcp-like structures in the liquid system, together with the indication of the presence of some complex tetrahedral structures at high pressures. We also observe that as the pressure increase, the maximum cluster size grows through the precipitation of the individual and small local cluster.

## Acknowledgments

The authors would like to acknowledge the contribution of the LIPI high performance computing facilities to obtaining the research results. The work was supported by a PDUPT research grant from the DRPM-KEMENRISTEKDIKTI in the fiscal year 2018, with contract No. 037/SP2H/LT/K7/KM/2018. We are also indebted to Prof. Shimojo and his lab members for the valuable discussion, and also to Dr Taufiq Widjanarko from Nottingham University for his input and suggestions.

## ORCID iDs

Rizal Arifin https://orcid.org/0000-0002-3917-9963
Muhammad Malyadi https://orcid.org/0000-0002-0419-3749
Ghulam Asrofi Buntoro https://orcid.org/0000-0001-5936-0359
Darminto https://orcid.org/0000-0002-6269-9246

## References

[1] Poole P H, Sciortino F, Essmann U and Stanley H E 1992 *Nature* **360** 324
[2] Mishima O and Stanley H E 1998 *Nature* **392** 164
[3] Koga K, Tanaka H and Zeng X C 2000 *Nature* **408** 564
[4] Errington J R and Debenedetti P G 2001 *Nature* **409** 318
[5] Koura A and Shimojo F 2008 *Phys. Rev.* B **78** 104203
[6] Fujita T, Konno K, Zhang W, Kumar V, Matsuura M, Inoue A, Sakurai T and Chen M W 2009 *Phys. Rev. Lett.* **103** 075502

[7] Fujita T, Guan P F, Sheng H W, Inoue A, Sakurai T and Chen M W 2010 *Phys. Rev.* B **81** 140204
[8] Pan M X, Wang J G, Yao Y S, Zhao D Q and Wang W H 2001 *J. Phys.: Condens. Matter.* **13** L589
[9] Sun Y, Zhang Y, Zhang F, Ye Z, Ding Z, Wang C Z and Ho K M 2016 *J. Appl. Phys.* **120** 015901
[10] Liu C S, Zhu Z G, Xia J and Sun D Y 2001 *J. Phys.: Condens. Matter* **13** 1873
[11] Waseda Y 1980 *The Structure of Non-Crystalline Materials* (New York: McGraw-Hill)
[12] Li G X, Liang Y F, Zhu Z G and Liu C S 2003 *J. Phys.: Condens. Matter* **15** 2259
[13] Jakse N and Pasturel A 2013 *Sci. Rep.* **3** 3135
[14] Hoshino K 2009 *J. Phys.: Condens. Matter* **21** 474212
[15] Wu S, Fang X W, Wang S Y, Wang C Z, Yao Y X, Yao Y X, Ho K M, Ding Z D and Chen L Y 2011 *J. Appl. Phys.* **110** 103518
[16] Saitoh K, Sato T and Shinke N 2006 *Mater. Trans.* **47** 742
[17] Jani J M, Leary M, Subic A and Gibson M A 2019 *Mater. Des.* **56** 1078
[18] Chu C L, Chung C Y, Lin P H and Wang S D 2004 *Mater. Sci. Eng.* A **366** 114
[19] Spuni M E and Brandis H F 2005 *Anal. Bioanal. Chem.* **381** 557
[20] Rokicki R, Hryniewicz T, Pulletikurthi C, Rokosz K and Munroe N 2015 *J. Mater. Eng. Perform.* **24** 1634
[21] Wadood A 2016 *Adv. Mater. Sci. Eng.* **2016** 4173138
[22] Plimpton S 1995 *J. Comput. Phys.* **117** 1
[23] Zhou X W, Johnson R A and Wadley H N G 2004 *Phys. Rev.* B **69** 144113
[24] Arifin R, Malyadi M, Munaji, Buntoro G A and Darminto 2019 *J. Phys.: Conf. Ser.* **1171** 012035
[25] Nosé S 1984 A molecular dynamics method for simulation in the canonical ensemble *Molec. Phys.* **52** 255
[26] Hoover W B 1985 Canonical dynamics: equilibrium phase-space distribution *Phys. Rev.* A **31** 1695
[27] Roux S L and Jund P 2010 *Comput. Mater. Sci.* **49** 70
[28] Stukowski A 2010 *Modelling Simul. Mater. Sci. Eng.* **18** 015012
[29] Lee G W, Gangopadhyay A K, Hyers R W, Rathz T J, Rogers J R, Robinson D S, Goldman A I and Kelton K F 2008 *Phys. Rev.* B **77** 184102
[30] Kelton K F, Lee G W, Gangopadhyay A K, Hyers R W, Rathz T J, Rogers J R, Robinson M B and Robinson D S 2003 *Phys. Rev. Lett.* **90** 195504
[31] Shenck T, Holland-Moritz D, Simonet V, Bellissent R and Herlach D M 2002 *Phys. Rev. Lett.* **89** 075507
[32] Mizuno A, Matsumura S, Watanabe M, Kohara S and Takata M 2005 *Mater. Trans.* **46** 2799
[33] Sheng H W, Ma E, Liu H Z and Wen J 2006 *Appl. Phys. Lett.* **88** 171906
[34] Xiong L H *et al* 2015 *Acta Mater.* **92** 102
[35] Ackland G J and Jones A P 2006 *Phys. Rev.* B **73** 054104

# Pressure dependence of the structure of liquid NiTi: a molecular dynamics study

ORIGINALITY REPORT

| 20% | 13% | 14% | 10% |
| --- | --- | --- | --- |
| SIMILARITY INDEX | INTERNET SOURCES | PUBLICATIONS | STUDENT PAPERS |

MATCH ALL SOURCES (ONLY SELECTED SOURCE PRINTED)

3%

★ www.mdpi.com

Internet Source

| | | | |
| --- | --- | --- | --- |
| Exclude quotes | Off | Exclude matches | Off |
| Exclude bibliography | Off | | |